ACCURACY PERFORMANCE OF SATELLITE-DERIVED SEA SURFACE TEMPERATURE PRODUCTS FOR THE INDONESIAN SEAS

***Restu TRESNAWATI*[1,5], *Anindya WIRASATRIYA*[2,4], *Adi WIBOWO*[3]**

DOI: 10.21163/GT_ 2022.172.07

ABSTRACT:
The precision of sea surface temperature (SST) from remote sensing data is essential to recognize SST fluctuations prompted by extreme weather conditions due to global climate warming, such as tropical cyclones (TCs). Since 1981 the active remote sensing of satellite-based SST measurements has been around and proliferating to date in Indonesia. However, there has not been much research on the validation of several remote sensing datasets in Indonesia's seas that has limited coverage of buoy observations. Moreover, no studies correspond to which data are the most precise in describing SST fluctuations in tropical storms. In this study, six remote sensing/satellite (Operational Sea Surface Temperature and Sea Ice Analysis (OSTIA), Regional Australian Multi-Sensor SST Analysis (RAMSSA), Global Australian Multi-Sensor SST Analysis (GAMSA), Microwave Infrared Optimally Interpolated (MWIROI), Multi-scale Ultra-high Resolution (MUR), and K10) data are validated and compared to analyze SST fluctuations in TC as a case study. The validation method uses the Haversine distance formula to reach the highest quality iQuam data with satellite data. The comparison analysis is performed by plotting the SST and wind slop in a TC area. Based on the validation, The OSTIA, RAMSSA, GAMSSA, and MWIROI datasets ranked in the top 4 of the smallest RMSEs with values < 0.5. Moreover, in the SST and wind slop in a TC area, TC affects SST cooling as detected in the MUR and K10 datasets where there is a decrease of > 2 ^{o}C. In the MWIROI, the decline is more noticeable significant > 3 ^{o}C.

Keywords: *Validation, Sea Surface Temperature, Remote Sensing, Tropical Cyclone*.

1. INTRODUCTION

SST is an essential and fundamental parameter in the global oceanic atmospheric system (Xu *et al.*, 2021; Xiao *et al.*, 2019). The SST is used to understand, monitor, and predict heat, gas flow, and momentum at various scales that define complicated interactions between the atmosphere and ocean (O'Carroll *et al.*, 2019; Small *et al.*, 2008). Currently, the global climate change is altering due to human activities, particularly those that generate the release of greenhouse gases from fossil energies (Mcmichael *et al.*, no date). Climate change has significantly affected marine, aquatic, and terrestrial lives. The most noticeable effect is the accumulation of heightened doses of carbon dioxide in the atmosphere, responsible for the greenhouse effect.

[1]*Faculty of Fisheries and Marine Sciences, Diponegoro University, 50275, Semarang, Indonesia, restutresnawati@students.undip.ac.id, etubowo@gmail.com*
[2]*Department of Oceanography, Faculty of Fisheries and Marine Sciences, Diponegoro University, 50275, Semarang, Indonesia, anindyawirasatriya@lecturer.undip.ac.id, aninosi@yahoo.co.id*
[3]*Department of Informatics, Faculty of Science and Mathematics, Diponegoro University, 50275, Semarang, Indonesia, bowo.adi@live.undip.ac.id*
[4]*Center for Coastal Rehabilitation and Disaster Mitigation Studies, Diponegoro University, 50275, Semarang, Indonesia*
[5]*Semarang Climatology Station, Indonesian Agency for Meteorology Climatology and Geophysics, 50145, Semarang, Indonesia*

The oceans have absorbed heat from greenhouse gas emissions, which contribute to the rising SST (Rhein *et al.*, 2013). SST changes can lead to extreme weather and natural disasters, such as droughts and floods, affecting various environmental conditions, dynamics (Herbert *et al.*, 2010), and tropical storms droughts (Upadhyay, 2020; Aboulnaga, Elwan and Elsharouny, 2019). Thus, recognizing SST fluctuations is the first step in detecting possible climate changes because the SST is an essential variable in climate change studies.

The accurate knowledge of the distribution and time changes of the SST is increasingly essential. Moreover, the SST is the first marine variable to be studied from Earth observation satellites and is easily measured by satellites and in situ sensors (Minnett *et al.*, 2019; Donlon *et al.*, 2007). Moreover, it is required as an input to forecasting systems to determine the modeling of ocean circulation and energy exchange (Donlon *et al.*, 2007).

The dynamic flow of satellite-based SST measures has been around since 1981 (Merchant *et al.*, 2019; O'Carroll *et al.*, 2019; Donlon *et al.*, 2007). Together with the general in situ measurements forming the modern era SST observation system, the numeral and variety of sensors have dramatically expanded and continued to rise (O'Carroll *et al.*, 2019; Martin, 2014). Prior satellite missions donating to the current and current constellation of SSTs have been described by (O'Carroll *et al.*, 2019). SST data were a mature component of observation systems in 1998 and data products with proven capabilities (Bell *et al.*, 2009). However, the availability of these products is limited to large datasets and is challenging to obtained in near real-time (NRT), (Donlon *et al.*, 2007; O'Carroll *et al.*, 2019), while the demand for SST data applications continues to grow.

The Global Ocean Data Assimilation Experiment (GODAE) has defined the minimum data specification for operational marine models as a solution to this problem (Bell *et al.*, 2009), Accordingly Group for High-Resolution Sea Surface Temperature (GHRSST previously, GODAE High-Resolution Sea Surface Temperature Pilot Project) was formed to address the specifications (Donlon *et al.*, 2009) for SST needs in the global coverage: a minimum spatial resolution of 10 km, updated every 6 hours and minimum accuracy of 0.2 ºC (Smith and Koblinsky, 2001).

The large volume of satellite information generated by GHRSST-Pilot Project (PP) requires, among other things, coordination between data providers (for each satellite sensor) and users, quality control (QC)and archiving methods, and data distribution tools (Robinson, 2004; Robinson, 2010). Jet Propulsion Laboratory (JPL)'s Physical Oceanography Distributed Active Archive Center (PO.DAAC) has developed infrastructure to fulfill the requirements of this project, including NRT (Armstrong *et al.*, 2011; Luquire, 2021). PO.DAAC has also been building a metadata repository since 1993, where the metadata for each L2P product are ingested into an externally accessible database through a web-based search (Armstrong, Bingham and Vazquez, 2004).

They were generated from a wide variety of data by the PO.DAAC as remote sensing SST validation is very important to determine the precision of SSTs in recognizing SST fluctuations in global warming and climate prediction (Hausfather *et al.*, 2017). The accuracy of SSTs from remote sensing data is one of the essential factors in climate and marine analysis (Sukresno, Jatisworo and Hanintyo, 2021). Validating daily remote sensing data with in situ data is required to bring high-quality remote sensing data.

In general, remote sensing SST validation is performed with data in situ measurements from buoys (Castro, Wick and Steele, 2016a; Hao *et al.*, 2017; Reddy *et al.*, 2018). Several studies on remote sensing SST data validation in Indonesia have been conducted (Irawan *et al.*, 2004; Sukresno *et al.*, 2018; Sukresno, Jatisworo and Hanintyo, 2021). However, due to Indonesian waters and limited buoy observation data, SST validation within the Indonesian seas is challenging. Furthermore, Indonesian waters/seas are considered essential as they have different SST characteristics in each region and are located between the Pacific and Indian Oceans, so they are semi-closed (Putra, Karang and Putra, 2019).

The validation of remote sensing SST data is important to determine the best dataset to be used in the Indonesian seas. Validations that have been performed generally only consider the general

state of data and very rarely focus on extreme events. In this study, we want to re-test whether validated data can capture extreme phenomena that quickly take place and whether there is a decrease in the SST caused by a TC event as a case in point. Datasets selected through validation tests and extreme phenomena are expected to describe a phenomenon and can be utilized in the analysis and prediction of extreme weather conditions.

In this study, six-remote sensing/satellite JPL PO.DAAC (Operational Sea Surface Temperature and Sea Ice Analysis (OSTIA), Regional Australian Multi-Sensor SST Analysis (RAMSSA), Global Australian Multi-Sensor SST Analysis (GAMSA), Microwave Infrared Optimally Interpolated (MWIROI), Multi-scale Ultra-high Resolution (MUR), and K10) data were validated. The validation method was carried out by comparing the highest quality iQuam data with satellite data using the Haversine distance formula. An analysis was conducted through an error approach, standard deviation, and bias, where most minor errors and bias values are expected. This study performed the earliest remote sensing SST data validation investigation to identify SST changes that occur due to extreme weather events, such as TCs. The validation and comparison analysis were deployed in an open-source Python language and available at https://github.com/bowoadi/sst-validation.

2. DATA AND METHODS

2.1. Data

2.1.1. Dataset SST

Six types of interpolated SST L4 analysis remote sensing datasets were used in this study in 2021 in the coordinates of Indonesia's territory with latitude –12º – 12º and longitude 91º – 147º. The data were acquired from the NASA's JPL Physical Oceanography Distributed Active Archive Center (http://podaac.jpl.nasa.gov). The daily dataset is presented in **Table 1**:

Table 1.

Satellite data L4 SST products.

No	Product Name	Spatial Resolution	Number of Data	Sensor
1	K10 (JPL), 2018)	0.1º	49.056.000	4, 7
2	MWIROI (Systems, 2017)	0.09º	60.555.392	5, 6, 8
3	OSTIA (UKMO, 2012)	0.054º	168.220.274	3, 4, 7, 8
4	RAMSSA (ABOM), 2019b)	0.083º	71.206.895	1, 2, 4
5	GAMSSA (ABOM), 2019a)	0.25º	7.848.960	1,2
6.	MUR (NASA/JPL, 2019)	0.25º	7.848.960	1, 2, 3, 5, 6

1= Buoys GTS 3= AVHRR NOAA 5= MODIS Aqua,Terra 7= Seviri
2= Ships GTS 4= AVHRR MetOp 6= WindSat 8= TMI TRMM

The Naval Oceanographic Office (NAVOCEANO) K10 SST operates satellite data only and merges L2 SST products in the presented average weight to describe the SST at a depth of 1 m, and this is one of the results of L4 that does not use the OI technique. All IR inputs are developed by NAVOCEANO using a separate nonlinear regression qualified against a control-powered GTS float buoy from the previous month. (May *et al.*, 1998).

MW data are excellent at capturing water levels with persistent turbidity where "the all-weather" MW sensor coverage improves accuracy. As shown (in the study by Brasnett (2008), MW and IR data contribute equal measure to the quality analysis for some of these analyses. Hence, the implementation (accuracy) of L4 products compared here, particularly those depending on MW data, is positively compromised.

The Remote Sensing System (REMSS) MWIR (MWIR) SST products use OI analysis and satellite data only (http://www.remss.com/measurements/sea-surface-temperature/oisst-description). Inputs are calibrated for daytime use using empirical heating models. The foundation SST product was initially designed for the National Hurricane Center to use the Statistical Hurricane Intensity Projection (SHIPS) model for considering storm intensity. (Castro, Wick and Steele, 2016b). The Operational Sea Surface Temperature and Sea Ice Analysis (OSTIA), (Brasnett, 2008) is assembled daily by the UK Met Office and is used as an operational boundary condition in the NWP and Digital Marine Forecasting in the Met Office and European Centre for Medium-Range Forecasting (ECMWF). OSTIA systems typically imported MW data from AMSR but have limited WindSat SST imports during period gaps using OI analysis. Input data are filtered to eliminate daytime observations with winds < 6 m/s to eliminate probable examples of daytime heating. Although provided at 0.05˚ (~ 6 km), the OSTIA SST grid is actually in an acceptable design (Donlon *et al.*, 2007).

In high-resolution operations, the Regional Australian Multi-Sensor Sea surface Australia temperature Analysis (RAMSA) has developed Bureau of Meteorology (BOM) within Australia's Blue-Ocean Ocean project. The new RAMSA system combines SST data from infrared and microwave sensors at spin to produce SST foundation estimates. The main difference between the RAMSA and other analyses of other SST foundation analyses are associated with RAMSA's methods for implementing advanced systems and determining weights for different data entry streams and bias edits, iFremer, and Met Office analysis systems among all. satellite input data using SST data from the Advanced Along Track Scanning Radiometer (AATSR), (Beggs *et al.*, 2011).

The BOM produces daily SST foundation analysis at a resolution of 0.25º as the Global Australian Multi-Sensor SST Analysis (GAMSSA). It is used as a boundary requirement in the global NWP system and is an extension of the regional L4 product 0.083º (Beggs *et al.*, 2011).

The Multi-scale Ultra-high Resolution (MUR) is produced daily by NASA's JPL. Unlike other outcomes that use standard OI techniques, the MUR system uses a statistical interpolation method based on wavelet analysis known as the multiresolution variation examination (Mallat, 1989). This multi-scale signal reconstruction technique is excellent for processing multiple spatial resolutions of L2 products used in different satellites' analysis and irregular swath patterns (Chin, Milliff and Large, 1998). The main contribution of this product is fit spatial resolution (horizontal) and the capability to handle high-resolution SST features such as fronts.

2.1.2. iQuam

iQuam is an in-situ dataset developed by the NOAA Center for Satellite Application and Research (STAR). Measurement data are obtained from ships, drifters, ARGO floats, and tropical mooring data. The data are been processed with strict quality control so that the in situ data obtained are reliable (Sukresno, Jatisworo and Hanintyo, 2021), as presented in **Fig. 1**. The present study used the iQuam dataset obtained from all measurements from ships, drifters, ARGO float, and tropical mooring data in 2021, with 156,152 datasets in total. The iQuam dataset is downloaded through the NOAA: https://www.star.nesdis.noaa.gov/sod/sst/iquam/data.html (accessed February 20, 2022). The iQuam dataset used in SST validation has a similar spatial distribution throughout the Indonesian seas.

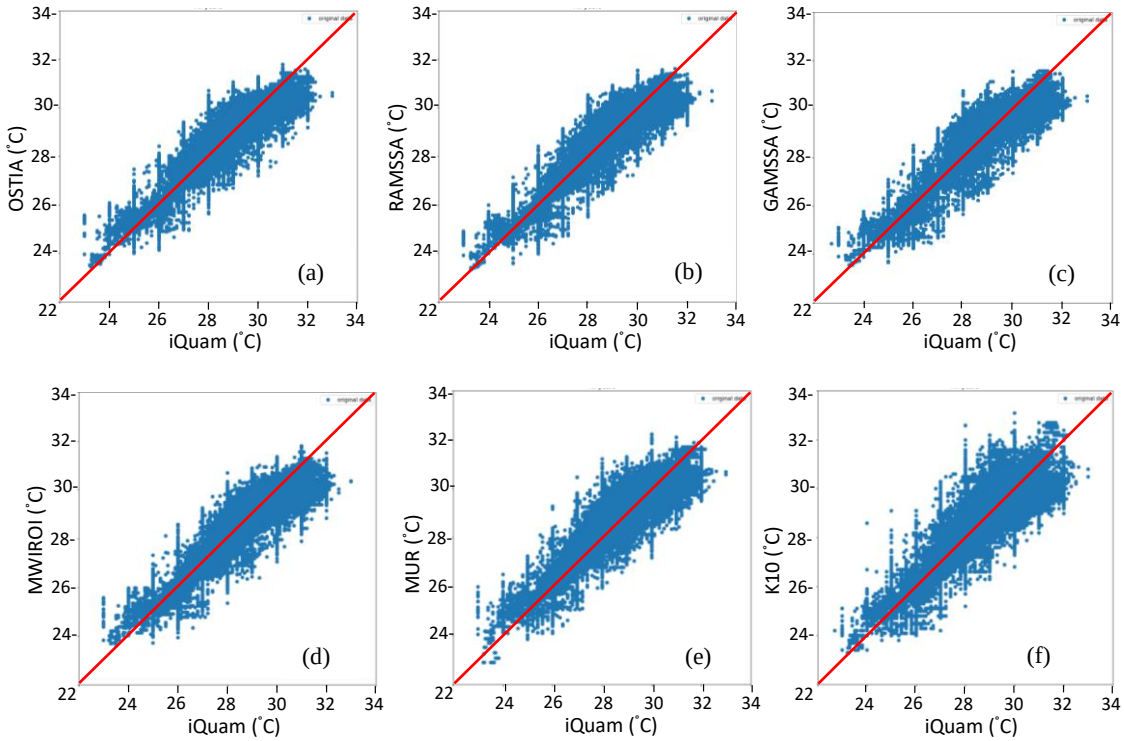

Fig. 1. Scatterplot among the six datasets against iQuam, a) OSTIA, b) RAMSSA, c) GAMSSA, d) MWIROI, e) MUR, f) K10.

2.1.3. Surface Wind

To comprehend the physical pressure of TCs, as an example of a case in the trial on the TC Seroja event, surface wind data from Cross Calibrated Multi-Platform (CCMP) version 2.0 grid analyzed surface winds between March 31 and April 15, 2021 were used. The CCMP used is a level 3 marine wind vector product produced from satellites, mooring buoys, and wind data models. The temporal and spatial resolutions of the surface wind data were 6 h and 0,25º × 0,25º. The CCMP accuracy is more elevated than other wind reanalysis data (Atlas *et al.*, 2011). This dataset can be downloaded from https://www.remss.com/measurements/ccmp/ (accessed February 25, 2022).

2.2. Methods

The extraction of six SST datasets was carried out in situ according to the data location iQuam at the same spot and time. The filtering process was performed by taking the highest-quality iQuam data. Each of the datasets was positioned with an iQuam dataset on the same acquisition day. The validation employs the Python program language with the following validation algorithm using the Haversine distance formula.

Input:

$\mathbf{P} = \{P_{0,0}, \dots, P_{n-1,m-1}\}, \quad P_{i,j} = (Px_i, Py_j, Pt_{i,j}), \quad i = 0,1 \dots, n-1,$
$j = 0,1 \dots, m-1$

$\mathbf{Q} = \{Q_0, \dots, Q_{K-1}\}, \quad Q_k = (Qx_k, Qy_k, Qt_k), \quad k = 0,1 \dots, K-1$

Process:

$\mathbf{T} = \{T_0, \dots, T_{K-1}\}, T_k = -1, \quad k = 0,1 \dots, K-1$

$k = 0$

For each $k < K$:

$lo = 0$
$hi = n$
While $lo < hi$ **do**: // Find leftmost value greater than or equal to Q_k in longitude
    $mid = ceil\_to\_integer(\frac{lo+hi}{2})$
    If $Px_{mid} < Qx_k$:
        $lo = mid + 1$
    Else:
        $hi = mid$
$\hat{x} = lo$
$lo = 0$
$hi = n$
While $lo < hi$ **do**: // Find leftmost value greater than or equal to Q_k in latitude
    $mid = ceil\_to\_integer(\frac{lo+hi}{2})$
    If $Py_{mid} < Qy_k$:
        $lo = mid + 1$
    Else:
        $hi = mid$
$\hat{y} = lo$
$lo = 0$
$hi = n$
While $lo < hi$ **do**: // Find rightmost value less than or equal to Q_k in longitude
    $mid = ceil\_to\_integer(\frac{lo+hi}{2})$
    If $Qx_k < Px_{mid}$:
        $hi = mid$
    Else:
        $lo = mid + 1$
$\check{x} = lo - 1$
$lo = 0$
$hi = m$
While $lo < hi$ **do**: // Find rightmost value less than or equal to Q_k in latitude
    $mid = ceil\_to\_integer(\frac{lo+hi}{2})$
    If $Qy_k < Py_{mid}$:
        $hi = mid$
    Else:
        $lo = mid + 1$
$\check{y} = lo - 1$
$d_{\hat{x},\hat{y}}$
$= 2 \cdot R$
$\cdot \arcsin\left(\sqrt{\sin\left(\frac{(Py_{\hat{y}} - Qy_k)}{2}\right)^2 + \cos(Qy_k) \cdot \cos(Py_{\hat{y}}) \cdot \sin\left(\frac{(Px_{\hat{x}} - Qx_k)}{2}\right)^2}\right)$

$ds_{min} = d_{\hat{x},\hat{y}}$
$t_{selected} = Pt_{\hat{x},\hat{y}}$
$d_{\hat{x},\check{y}}$
$= 2 \cdot R$
$\cdot \arcsin\left(\sqrt{\sin\left(\frac{(Py_{\hat{y}} - Qy_k)}{2}\right)^2 + \cos(Qy_k) \cdot \cos(Py_{\hat{y}}) \cdot \sin\left(\frac{(Px_{\check{x}} - Qx_k)}{2}\right)^2}\right)$

If $ds_{min} > d_{\hat{x},\hat{y}}$:

$ds_{min} = d_{\hat{x},\hat{y}}$

$t_{selected} = Pt_{\hat{x},\hat{y}}$

$$d_{\check{x},\hat{y}} = 2 \cdot R \cdot \arcsin\left(\sqrt{\sin\left(\frac{(Py_{\check{y}} - Qy_k)}{2}\right)^2 + \cos(Qy_k) \cdot \cos(Py_{\check{y}}) \cdot \sin\left(\frac{(Px_{\hat{x}} - Qx_k)}{2}\right)^2}\right)$$

If $ds_{min} > d_{\check{x},\hat{y}}$:

$ds_{min} = d_{\check{x},\hat{y}}$

$t_{selected} = Pt_{\check{x},\hat{y}}$

$$d_{\check{x},\check{y}} = 2 \cdot R \cdot \arcsin\left(\sqrt{\sin\left(\frac{(Py_{\check{y}} - Qy_k)}{2}\right)^2 + \cos(Qy_k) \cdot \cos(Py_{\check{y}}) \cdot \sin\left(\frac{(Px_{\check{x}} - Qx_k)}{2}\right)^2}\right)$$

If $ds_{min} > d_{\check{x},\check{y}}$:

$ds_{min} = d_{\check{x},\check{y}}$

$t_{selected} = Pt_{\check{x},\check{y}}$

$k = k + 1$

P *is the SST satellite data that contain matrix data structures* $n \times m$ *with value* $P_{i,j} = (Px_i, Py_j, Pt_{i,j}),\ i = 0,1 \dots, n-1,\ j = 0,1 \dots, m-1$, *where* Px_i *is the longitude on the line to-i,* Py_j *is latitude in the column to-j, and* $Pt_{i,j}$ *is the SST on the line to-i and column to-j. The values* Px *and* Py *have been sorted.*

Q *is the high-quality iQuam data that contain a flat-array data structure with a size K and value* $Q_k = (Qx_k, Qy_k, Qt_k),\ k = 0,1 \dots, K-1$, *where* Qx_k *is the longitude on the array to-k,* Qy_k *is the latitude on the array to-k, and* Qt_k *is the SST on the array to-k.*

R *is the estimated radius used in the calculation of distance between points using the formula Haversine distance, which has a value of 6373.*

Iterations were performed for each k. The point closest to Q_k, was determined based on four conditions, namely, leftmost point with value Px_i (more than the same as Qx_k as $\hat{x}$), leftmost point with value Py_i (more than the same as Qy_k as $\hat{y}$), the rightmost point with the value Px_i (less than the same as Qx_k as $\check{x}$), and the rightmost point with value Py_i (less than the same as Qy_k as $\check{y}$). Then the four conditions were combined into four points, namely $\{(\hat{x},\hat{y}), (\check{x},\hat{y}), (\check{x},\hat{y}), (\check{x},\check{y})\}$ each calculated with distance Qx_k and Qy_k. Then the one that has the shortest distance was selected. The difference in the SST value was obtained by reducing the Qt_k value with SST satellite value from the point with the shortest distance.

2.2.1. RMSE, Standard Deviation, and Bias

Statistical testing to witness the proximity of remote sensing data to iQuam was conducted using RMSE, standard deviation, and bias. The smallest value indicates a better error with observational data (Hidalgo García, 2021).

$$RMSE = \sqrt{\frac{1}{n}\sum_{i=1}^{n}(SST\ In\ Situ_i - SST\ Satelit_i)^2} \quad (1)$$

3. RESULTS AND DISCUSSION

3.1. SST Dataset Validation

The initial comparison of six-satellite datasets against the iQuam dataset was carried out by displaying the plot scatter of the six data on 2021 presented in **Fig. 1** and daily data distribution that describes the state of remote sensing and iQuam sorted according to the smallest RMSE values as presented in **Table 2**. Data adjacent to diagonal lines indicates a good distribution of data, as can be seen from root mean square error (RMSE) and slight standard deviation. RMSE, standard deviation, and bias are shown in **Table 2** in the order from the smallest RMSE values. OSTIA has the smallest RMSE and standard deviation values with 0.425 and 0.461, respectively. MUR has the lowest bias value with 0.045.

Table 2.

RMSE values, standard deviations, and biases of six datasets against iQuam.

No	Name	RMSE	Standard Dev	Bias
1	OSTIA	0.425	0.461	–0.079
2	RAMSSA	0.451	0.488	–0.073
3	GAMSSA	0.454	0.489	–0.076
4	MWIROI	0.471	0.529	–0.143
5	MUR	0.516	0.541	0.045
6	K10	0.620	0.648	–0.078

Remote sensing data with an RMSE value of < 0.5 were taken to show the error distribution. The results of the spatial error value interpretation are presented in **Fig. 2**. All Indonesian seas have a reasonably acceptable error value, ranging from –0.5 to 0.5, symbolized by a bluish-green color. However, the error value is quite significant, ranging from 1 to 2 among the Karimata Strait, Makassar Strait, and around the Aru Sea.

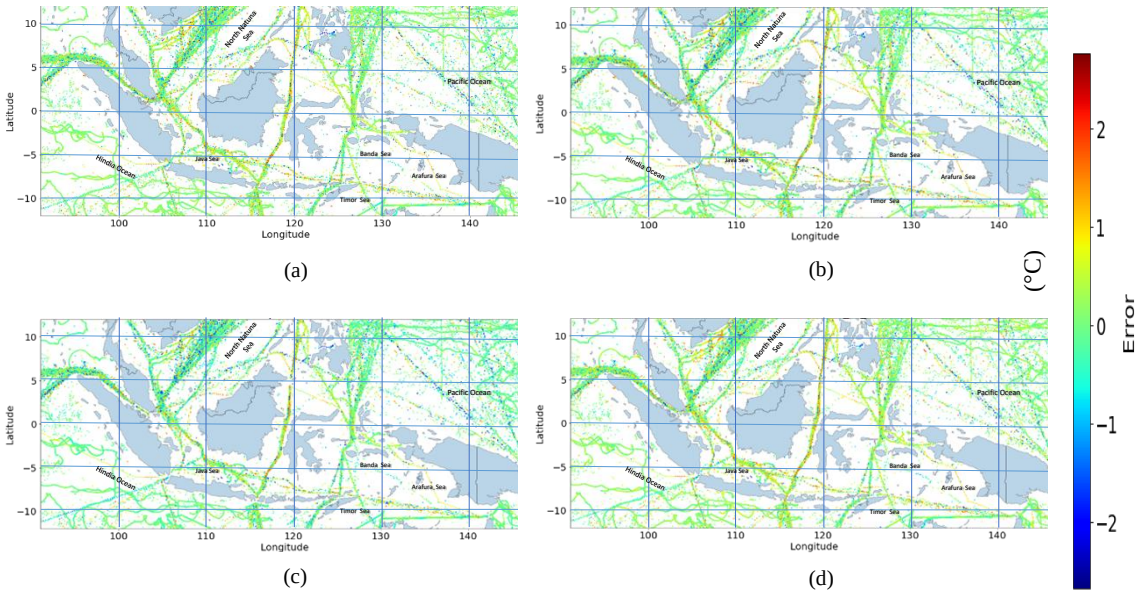

Fig. 2. Distribution of error values in 2021 across Indonesian territorial waters a) OSTIA, b) RAMSSA, c) GAMSSA, and d) MWIROI.

The validation tests concluded that the selected datasets with RMSE values and minor standard deviations were owned on the OSTIA, RAMSSA, GAMSSA, and MWIROI datasets. Similarly, by proving the distribution of error values in 2021, shown in **Fig. 2**, the four datasets have a reasonably small error value in almost all areas of Indonesian waters ranging from –0.5 to 0.5.

3.2. Sensitivity Tests for Extreme Weather Events

Although Indonesia is an equatorial tropical country, TC events occur pretty often as will be stated in the discussion below. From 2010 to 2021, at least five TCs have had quite an impact on Indonesia. In the previous discussion, the validation results of the six datasets were well known. Nonetheles, we also wanted to know how each SST dataset responded to TC events and whether each dataset captured an extreme weather phenomenon that quickly took place.

The SST is a critical factor in the supply of energy for a TC or storm and affects not only its formation (Gray, 1968; Gray, 1975; Emanuel, 1986; Wang *et al.*, 2007) but also the trace and intensity of the TC (Emanuel, 1999; Schade and Emanuel, 1999; Mei *et al.*, 2015). Even if atmospheric conditions are promising, TC will not develop if the SST is low (Lin *et al.*, 2008) and difficult to occur in SSTs < 26 ºC (Emanuel, 2003). In the ocean region bordering the Indonesian seas, especially in the southeastern part of the tropical Indian Ocean, several TCs have occurred, such as Anggrek (October 31 – November 4, 2010), Bakung (December 10 – 13, 2014), Cempaka (November 25 – 27, 2017), Dahlia (November 27 – December 2, 2017), (Paterson, 2012; Gutro, 2014; Samodra *et al.*, 2020; Yang *et al.*, 2020; Aditya *et al.*, 2021) and Seroja ; Latos *et al.*, 2022). TC events can cause critical oceanic phenomena in the form of cooling SSTs (Hazelworth, 1968; Stramma, Cornillon and Price, 1986; Leipper, 1967; Lin *et al.*, 2013). According to (Yang *et al.*, 2020) the effect of TCs on the oceans has changed the thermal stratification of the upper part of the oceans in the southeastern part of the tropical Indian Ocean by decreasing the SST (> 1.5 ºC). This paper also sees a decrease in SSTs for TC events in Malakas, Megi, and Chaba (Li *et al.*, 2020), but no studies have specified which remote sensing/satellite data are the most precise in describing SST fluctuations in tropical storm.

As a case study, this research will be indicating the development of TC Seroja using several plot areas on the TC development based on wind and SST data presented in **Figs. 3, 4** and **5**. As shown in **Fig. 3**, on April 1, a strong east wind appeared around the eastern island of Timor. On April 3, wind speeds increased by > 18 m/s in the Sawu Sea (SS) and Northern Australia. The existence of wind patterns on April 3 is the initial stage of the development of TC Seroja, with wind speeds of approximately about 18 – 20 m/s. The cyclone wind speed of > 23 m/s in the core eye of the TC indicates that TC Seroja fully developed on April 4 and lasted until April 6, 2021. These finding are in line with research (result of Setiawan *et al.*, 2021).

The Validation of six datasets in the TC Seroja case study was also observed through the SST plotting with the wind (**Fig. 4**). SST heating can be an early sign of a fast-paced TC event (65). The heating SST of > 30.5 ºC occurred since March 28, 2021, on almost all datasets. Although the heating is quite extreme, an SST 30.8 ºC occurred in the K10 and MUR datasets on March 28 – 30, but the dataset could describe the SST condition, which was quite extreme at the time of the full TC development. An increase in the wind speed can cool the surface air temperature during the TC development. The effect of wind occurring in extremes on April 2 – 8, 2021, as explained in **Fig. 4**, along with the decline in SSTs, was very noticeable until the SST reached > 1.5 ºC in the MWIROI and MUR datasets, whereas in the other datasets (OSTIA, RAMSSA, GAMSSA, and K10), the SST decrease when wind speed increase was relatively not very noticeable and tend to take place more slowly. Hence, when the wind weakened, the SST of the other datasets only decreased, which is an unnatural thing.

The SST cooling event that occurred during the full development of the TC on April 4 – 6, 2021 is presented in **Fig. 5** to detect the precision of remote sensing SST datasets against TC extreme events. The SST maps, SST temperature and wind line in a latitude of –11 º are shown for comparison.

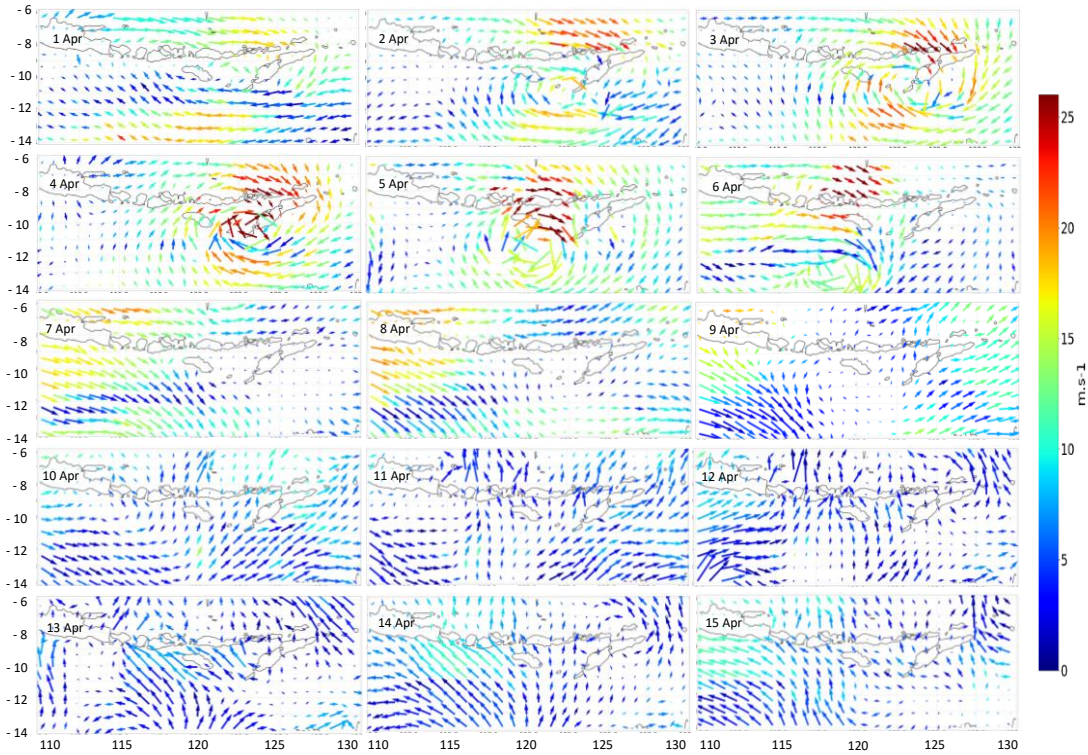

Fig. 3. Wind speed (m/s) on April 1 – 15, 2021.

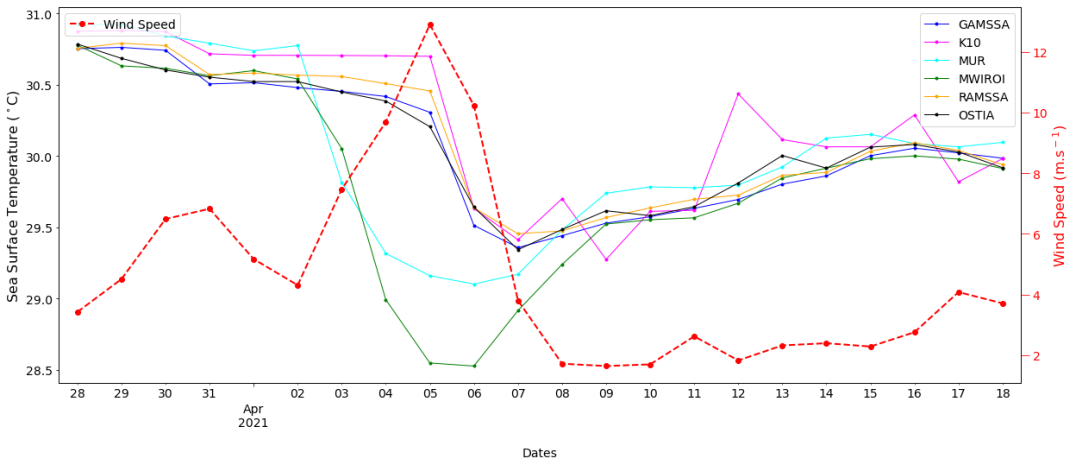

Fig. 4. Time series of the six datasets SST and wind speed of the Savu Sea on March 28 – Apr 31, 2021, (average area is 121 – 125°E; 8 – 11°S similar with the research finding in *Setiawan et al., 2021*.

The strong effect of TC Seroja as presented in **Fig. 5** (top) shows the decrease in the SST in almost all remote sensing data. The wind effect **Fig. 5** (bottom) shown with a slop line during the full TC formation can cause the cooling of SST, as an identification of the precision of remote sensing SST six datasets along with the increase in the wind during the full formation of TC Seroja on April 4 – 6, 2021. On April 4, 2021, a maximum wind speed of approximately > 15 m/s occurred in the longitude 122.5° – 123°, along with a more noticeable decline in SSTs in the MWIROI and MUR datasets.

By contrast, in the other four datasets, the decline in the SSTs is not very noticeable. On April 5, 2021, the maximum wind speed increased to > 22.5 m/s, including the strong gale on the Beaufort scale. Moreover, a relatively sharp decrease in SSTs was observed in the MWIROI and MUR datasets, where there is a drop until 3 ºC.

As presented in **Fig. 5** the traces of cyclones of the MUR and K10 datasets are visible on April 5 – 6, 2021, with cold SSTs ranging from 28 ºC to 29 ºC. OSTIA, RAMSSA, and GAMSSA almost look the same, but the traces of cyclones are not very clear. Meanwhile, in the MWIROI dataset, a visible TC travel since April 4 is characterized by the cold SST ranging of 27.5 ºC – 28.5 ºC. On April 6, 2021, a maximum wind speed of up to 25 m/s for the decrease in the SST that occurred due to strong winds was most visible in the MWIROI dataset where there was a decrease to > 3 ºC from 31.5 ºC to 28 ºC. Despite the RMSE value, MWIROI's standard deviation and bias are not the smallest but can better describe the state of the TC, especially at the time of its full development.

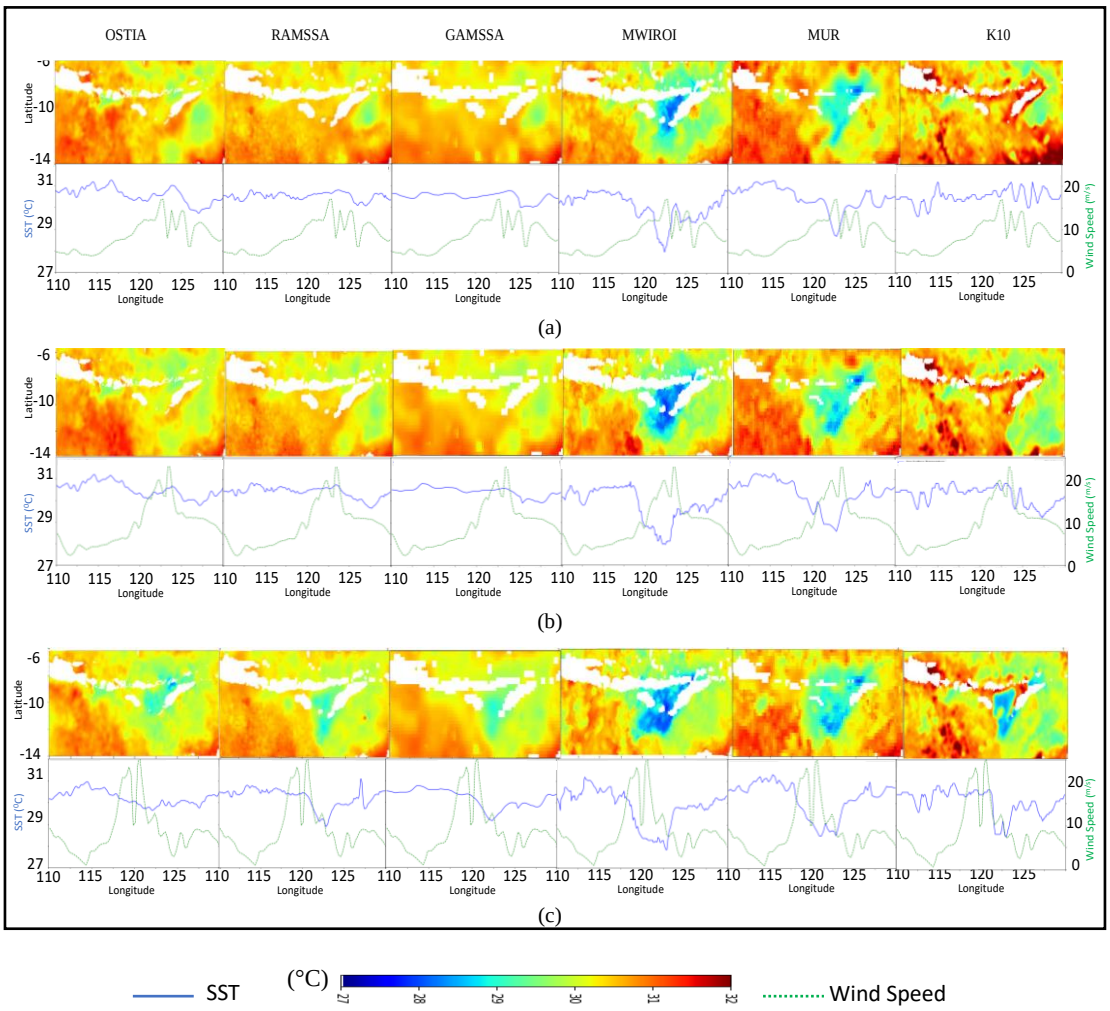

Fig. 5. Plotting SST (ºC) (top), SST (ºC) and wind (m/s) slope line in latitude of –11º (bottom) in at the time of full TC development; a) April 4, b) April 5 and c) April 6, 2021.

Increased wind speeds from April 3 to 7 and the disappearance of winds toward the southwest can cool the SST, (**Fig. 4** and **5)**.

Many factors can describe the total growth and development of TC Seroja in addition to the wind and SST. However, such formations fall outside the scope of this study, which focused on validating the remote sensing SST dataset against iQuam to detect TC Seroja events.

The most visible cyclone trail is shown by MWIROI and MUR, where the decrease in the SST is evident from April 4 to 6, 2021. However, in the OSTIA, RAMSSA, and GAMSSA datasets, the decline in the SST is not very significant, which this happens because both have the same sensor, specifically MODIS Aqua and Terra. The twin-MODIS design aims aimed to optimize cloud-free imaging while minimizing the optical effects of shadows and glares that occur with morning and afternoon sunlight. In three different resolutions, i.e., 250 m, 500 m, and 1 km, MODIS data products help improve our understanding of global environmental processes and dynamics occurring on the land, oceans, and lower atmosphere. The MODIS data records help extend heritage data, such as NOAA's Advanced Very High-Resolution Radiometer, thus ensuring the critical continuity of such collections to support our investigations of short- and long-term global environmental changes. MODIS-derived data products continue to play a vital role in helping develop and validate global Earth system models with sufficient predictive potential to inform and help policymakers address global environmental changes.

The MWIROI dataset is relatively undisturbed by the cloud cover due to the combination of IR data with microwave data that can penetrate the cloud. (Li et al., 2020). In expansion, because this product was initially developed to estimate hurricane intensity, it may be better to capture SST-related ocean extreme events.

4. CONCLUSIONS

In this study, six remote sensing/satellite datasets (OSTIA, RAMSSA, GAMSA, MWIROI, MUR and K10) were validated and compared to analyze and validate investigations to identify SST changes that occur due to extreme weather events, such as TCs. The validation method was performed by comparing the highest-quality of iQuam data with satellite data using the Haversine distance formula. The comparison analysis was performed by plotting the SST slope in a TC area. Based on the validation, the OSTIA, RAMSSA, GAMSSA, and MWIROI datasets ranked in the top 4 with the smallest RMSE with a value i.e., < 0.5. Moreover, in a TC area, the TC Seroja wind speed increased by > 22.5 m/s on April 5, 2021, and SST cooling was detected in the MUR and K10 datasets denoted by a decrease of > 2 ºC. For MWIROI, the decline was more noticeably significant as > 3 ºC. This finding shows that the MWIROI dataset can describe the extreme conditions of TC Seroja better than other datasets. The most visible cyclone trail is shown by MWIROI and MUR, where the decrease in the SST is highly evident from April 4 to 6, 2021. This happens because both have the same sensor, specifically MODIS Aqua,Terra and WindSat. The twin-MODIS design aim to optimize cloud-free imaging while minimizing the optical effects of shadows and glare that occur with morning and afternoon sunlight. The cyclone's footprint was the most pronounced in MWIROI with a resolution of 0.09º because the product was initially designed to estimate storm intensity. This dataset can be used in future studies, especially for extreme weather or climate analysis.

ACKNOWLEDGMENTS

The authors would like to thank you for the support from PUSDIKLAT BMKG and Diponegoro University. SST L4 analysis remote sensing datasets available at NASA Jet Propulsion Laboratory Physical Oceanography Distributed Active Archive Center (PODAAC, http://podaac.jpl.nasa.gov). iQuam is an in-situ dataset developed by the NOAA Center for Satellite Application and Research (STAR) available at https://www.star.nesdis.noaa.gov/sod/sst/iquam/data.html
CCMP Version-2.0 vector wind from https://www.remss.com/measurements/ccmp/

REFERENCES

(ABOM), A. B. O. M. (2019a) 'GHRSST Level 4 GAMSSA_28km Global Foundation Sea Surface Temperature Analysis v1.0 dataset (GDS2)'. NASA Physical Oceanography DAAC. doi: 10.5067/GHGAM-4FA1A.

(ABOM), A. B. O. M. (2019b) 'GHRSST Level 4 RAMSSA_9km Australian Regional Foundation Sea Surface Temperature Analysis v1.0 dataset (GDS2)'. NASA Physical Oceanography DAAC. doi: 10.5067/GHRAM-4FA1A.

(JPL), N. J. P. L. (2018) 'GHRSST Level 4 K10_SST Global 10 km Analyzed Sea Surface Temperature from Naval Oceanographic Office (NAVO) in GDS2.0'. NASA Physical Oceanography DAAC. doi: 10.5067/GHK10-L4N01.

Aboulnaga, M. M., Elwan, A. F. and Elsharouny, M. R. (2019) 'Global Climate Change Risks: Sectors and Variables' Changes', in *Urban Climate Change Adaptation in Developing Countries*. Springer, pp. 19–48.

Aditya, H. N. *et al.* (2021) 'Impact of tropical Cyclones Cempaka and Dahlia to the variability of chlorophyll-a and sea surface temperature in the Seas Southern Coast of Java Island', 27.

Armstrong, E. ~M., Bingham, A. and Vazquez, J. (2004) 'Managing global satellite data: The GHRSST-PP', in *AGU Fall Meeting Abstracts*, pp. SF33B-07.

Armstrong, E. M. *et al.* (2011) 'Report on the Global Data Assembly Center (GDAC) to the 12th GHRSST Science Team Meeting'.

Atlas, R. *et al.* (2011) 'A cross-calibrated, multiplatform ocean surface wind velocity product for meteorological and oceanographic applications', *Bulletin of the American Meteorological Society*, 92(2), pp. 157–174.

Beggs, H. *et al.* (2011) 'RAMSSA - An operational, high-resolution, Regional Australian Multi-Sensor Sea surface temperature Analysis over the Australian region', *Australian Meteorological and Oceanographic Journal*, 61(1), pp. 1–22. doi: 10.22499/2.6101.001.

Bell, M. J. *et al.* (2009) 'GODAE: The Global Ocean Data Assimilation Experiment', *Oceanography*, 22(3), pp. 14–21. Available at: http://www.jstor.org/stable/24860986 (Accessed: 23 April 2022).

Brasnett, B. (2008) 'The impact of satellite retrievals in a global sea-surface-temperature analysis', (August), pp. 1745–1760. doi: 10.1002/qj.319.

Castro, Wick and Steele (2016a) 'Validation of satellite sea surface temperature analyses in the Beaufort Sea using UpTempO buoys', *Remote Sensing of Environment*, 187, pp. 458–475.

Castro, Wick and Steele (2016b) 'Validation of satellite sea surface temperature analyses in the Beaufort Sea using UpTempO buoys', *Remote Sensing of Environment*, 187, pp. 458–475. doi: 10.1016/j.rse.2016.10.035.

Chin, T. M., Milliff, R. F. and Large, W. G. (1998) 'Basin-scale, high-wavenumber sea surface wind fields from a multiresolution analysis of scatterometer data', *Journal of Atmospheric and Oceanic Technology*, 15(3), pp. 741–763. doi: 10.1175/1520-0426(1998)015<0741:BSHWSS>2.0.CO;2.

Donlon, C. *et al.* (2007) 'The global ocean data assimilation experiment high-resolution sea surface temperature pilot project', *Bulletin of the American Meteorological Society*, 88(8), pp. 1197–1214.

Donlon, C. J. *et al.* (2009) 'The GODAE high-resolution sea surface temperature pilot project', *Oceanography*, 22(3), pp. 34–45.

Emanuel, K. (2003) 'Tropical cyclones', *Annual Review of Earth and Planetary Sciences*, 31(1), pp. 75–104.

Emanuel, K. A. (1986) 'An air-sea interaction theory for tropical cyclones. Part I: Steady-state maintenance', *Journal of Atmospheric Sciences*, 43(6), pp. 585–605.

Emanuel, K. A. (1999) 'Thermodynamic control of hurricane intensity', *Nature*, 401(6754), pp. 665–669.

Gray, W. M. (1968) 'Global view of the origin of tropical disturbances and storms', *Monthly Weather Review*, 96(10), pp. 669–700.

Gray, W. M. (1975) *Tropical cyclone genesis*. Colorado State University. Libraries.

Hao, Y. *et al.* (2017) 'Validation of MODIS sea surface temperature product in the coastal waters of the Yellow Sea', *IEEE Journal of Selected Topics in Applied Earth Observations and Remote Sensing*, 10(5), pp. 1667–1680.

Hausfather, Z. *et al.* (2017) 'Assessing recent warming using instrumentally homogeneous sea surface temperature records', *Science Advances*, 3(1). doi: 10.1126/sciadv.1601207.

Hazelworth, J. B. (1968) 'Water temperature variations resulting from hurricanes', *Journal of Geophysical Research*, 73(16), pp. 5105–5123.

Herbert, T. D. *et al.* (2010) 'Tropical ocean temperatures over the past 3.5 million years', *Science*, 328(5985), pp. 1530–1534. doi: 10.1126/science.1185435.

Hidalgo García, D. (2021) 'Analysis and precision of the Terrestrial Surface Temperature using Landsat 8 and Sentinel 3 images: Study applied to the city of Granada (Spain)', *Sustainable Cities and Society*, 71, p. 102980. doi: https://doi.org/10.1016/j.scs.2021.102980.

Irawan *et al.* (2004) 'STUDI PERBAND. SUHU PERMUKAAN LAUT MENGG. CITRA SATELIT NOAA-AVHRR (Faried Irawan)'.

Latos, B. *et al.* (2022) 'The role of tropical waves in the genesis of Tropical Cyclone Seroja-one of the first tropical cyclones to significantly impact Indonesian land'.

Leipper, D. F. (1967) 'Observed ocean conditions and Hurricane Hilda, 1964', *Journal of the Atmospheric Sciences*, 24(2), pp. 182–186.

Li, J. *et al.* (2020) 'Accurate evaluation of sea surface temperature cooling induced by typhoons based on satellite remote sensing observations', *Water (Switzerland)*, 12(5), pp. 1–16. doi: 10.3390/w12051413.

Lin, I.-I. *et al.* (2013) 'An ocean coupling potential intensity index for tropical cyclones', *Geophysical Research Letters*, 40(9), pp. 1878–1882.

Lin, I. I. *et al.* (2008) 'Upper-ocean thermal structure and the western North Pacific category 5 typhoons. Part I: Ocean features and the category 5 typhoons' intensification', *Monthly Weather Review*, 136(9), pp. 3288–3306.

Luquire, K. (2021) 'A Group for High Resolution Sea Surface Temperature (GHRSST) Level 4 sea surface temperature analysis produced as a retrospective dataset (four day latency) and near-real-time dataset (one day latency) at the JPL Physical Oceanography DAAC using wavelets '. Edited by N. C. for E. I. (U.S.). (NOAA Technical Information Series NESDIS DSMR ; 00266). doi: https://doi.org/10.25923/d47d-0413.

Mallat, S. G. (1989) 'A theory for multiresolution signal decomposition: the wavelet representation', *IEEE Transactions on Pattern Analysis and Machine Intelligence*, 11(7), pp. 674–693. doi: 10.1109/34.192463.

Martin, S. (2014) *An introduction to ocean remote sensing*. Cambridge University Press.

May, D. A. *et al.* (1998) 'Operational Processing of Satellite Sea Surface Temperature Retrievals at the Naval Oceanographic Office', *Bulletin of the American Meteorological Society*, 79(3), pp. 397–407. doi: 10.1175/1520-0477(1998)079<0397:OPOSSS>2.0.CO;2.

Mcmichael, A. J. *et al.* (no date) 'Chapter 20 Global climate change'.

Mei, W. *et al.* (2015) 'Northwestern Pacific typhoon intensity controlled by changes in ocean temperatures', *Science advances*, 1(4), p. e1500014.

Merchant, C. J. *et al.* (2019) 'Satellite-based time-series of sea-surface temperature since 1981 for climate applications', *Scientific data*, 6(1), pp. 1–18.

Minnett, P. J. *et al.* (2019) 'Half a century of satellite remote sensing of sea-surface temperature', *Remote Sensing of Environment*, 233, p. 111366. doi: https://doi.org/10.1016/j.rse.2019.111366.

NASA/JPL (2019) 'GHRSST Level 4 MUR 0.25deg Global Foundation Sea Surface Temperature Analysis (v4.2)'. NASA Physical Oceanography DAAC. doi: 10.5067/GHM25-4FJ42.

O'Carroll, A. G. *et al.* (2019) 'Observational needs of sea surface temperature', *Frontiers in Marine Science*, 6(JUL). doi: 10.3389/fmars.2019.00420.

Paterson, L. (2012) 'Tropical Low AU1011_01U (Anggrek)', *Bur. Meteorology. Australia. Accessed*, (November 2010).

Putra, I. N. J. T., Karang, I. W. G. A. and Putra, I. D. N. N. (2019) 'Analisis Temporal Suhu Permukaan Laut di Perairan Indonesia Selama 32 Tahun (Era AVHRR)', *Journal of Marine and Aquatic Sciences*, 5, pp. 234–236.

R. Gutro (2014) 'Bakung (Southern Indian Ocean)'. NASA's Goddard Space Flight Center. USA. Available at: https://www.nasa.gov/content/goddard/bakung-southern-indian-ocean/.

Reddy, B. *et al.* (2018) 'Comparison of AMSR-2 wind speed and sea surface temperature with moored buoy observations over the Northern Indian Ocean', *Journal of Earth System Science*, 127(1), pp. 1–11.

Rhein, M. *et al.* (2013) 'Observations: Ocean in Climate Change 2013: The Physical Science Basis. Contribution of Working Group I to the Fifth Assessment Report of the Intergovernmental Panel on Climate Change', *Fifth assessment report of the Intergovernmental Panel on Climate Change*, pp. 255–316.

Robinson, I. S. (2004) *Measuring the oceans from space: the principles and methods of satellite oceanography*. Springer Science \& Business Media.

Robinson, I. S. (2010) *Discovering the Ocean from Space: The unique applications of satellite oceanography*. Springer Science \& Business Media.

Samodra, G. *et al.* (2020) 'Frequency–magnitude of landslides affected by the 27–29 November 2017 Tropical Cyclone Cempaka in Pacitan, East Java', *Journal of Mountain Science*, 17(4), pp. 773–786. doi: 10.1007/s11629-019-5734-y.

Schade, L. R. and Emanuel, K. A. (1999) 'The ocean's effect on the intensity of tropical cyclones: Results from a simple coupled atmosphere--ocean model', *Journal of the atmospheric sciences*, 56(4), pp. 642–651.

Setiawan, R. Y., Susanto, R Dwi, *et al.* (2021) 'Impacts of tropical cyclone Seroja on the phytoplankton chlorophyll-a and sea surface temperature in the Savu Sea, Indonesia', *IEEE Access*, 9, pp. 152938–152944.

Setiawan, R. Y., Susanto, R. Dwi, *et al.* (2021) 'Impacts of Tropical Cyclone Seroja on the Phytoplankton Chlorophyll-a and Sea Surface Temperature in the Savu Sea, Indonesia', *IEEE Access*, 9, pp. 152938–152944. doi: 10.1109/ACCESS.2021.3125605.

Small, R. J. d *et al.* (2008) 'Air--sea interaction over ocean fronts and eddies', *Dynamics of Atmospheres and Oceans*, 45(3–4), pp. 274–319.

Smith, N. R. and Koblinsky, C. (2001) 'The ocean observing system for the 21st Century, a consensus statement', *Observing the Oceans in the 21st Century*, pp. 1–25.

Stramma, L., Cornillon, P. and Price, J. F. (1986) 'Satellite observations of sea surface cooling by hurricanes', *Journal of Geophysical Research: Oceans*, 91(C4), pp. 5031–5035.

Sukresno, B. *et al.* (2018) 'Three-Way Error Analysis of Sea Surface Temperature (Sst) Between Himawari-8, Buoy, and Mur Sst in Savu Sea', *International Journal of Remote Sensing and Earth Sciences (IJReSES)*, 15(1), p. 25. doi: 10.30536/j.ijreses.2018.v15.a2855.

Sukresno, B., Jatisworo, D. and Hanintyo, R. (2021) 'Validation of Sea Surface Temperature from GCOM-C Satellite Using iQuam Datasets and MUR-SST in Indonesian Waters', *Indonesian Journal of Geography*, 53(1), pp. 136–143. doi: 10.22146/IJG.53790.

Systems, R. S. (2017) 'GHRSST Level 4 MW_IR_OI Global Foundation Sea Surface Temperature analysis version 5.0 from REMSS'. PO. DAAC Pasadena, CA, USA.

UKMO (2012) 'GHRSST Level 4 OSTIA Global Foundation Sea Surface Temperature Analysis (GDS version 2)'. NASA Physical Oceanography DAAC. doi: 10.5067/GHOST-4FK02.

Upadhyay, R. K. (2020) 'Markers for Global Climate Change and Its Impact on Social, Biological and Ecological Systems: A Review', *American Journal of Climate Change*, 09(03), pp. 159–203. doi: 10.4236/ajcc.2020.93012.

Wang, G. *et al.* (2007) 'Tropical cyclone genesis over the South China Sea', *Journal of Marine Systems*, 68(3–4), pp. 318–326.

Xiao, C. *et al.* (2019) 'Short and mid-term sea surface temperature prediction using time-series satellite data and LSTM-AdaBoost combination approach', *Remote Sensing of Environment*, 233, p. 111358. doi: https://doi.org/10.1016/j.rse.2019.111358.

Xu, Z. *et al.* (2021) 'Long-term evolution of global sea surface temperature trend', *International Journal of Climatology*.

Yang, Y. *et al.* (2020) 'Diurnal Sea surface temperature response to tropical cyclone Dahlia in the Eastern tropical Indian Ocean in 2017 revealed by the Bailong buoy', *Dynamics of Atmospheres and Oceans*, 92, p. 101163.